2.1 Tensile Properties of Unidirectional CVI SIC/SIC Minicomposites with a Multilayer interphase and Near-Stoichiometric SIC Fibers

— K. Ozawa,* Y. Katoh, L.L. Snead (Oak Ridge National Laboratory), T. Nozawa, H. Tanigawa (Japan Atomic Energy Agency)

OBJECTIVE

The tensile behaviors of unirradiated unidirectional single tow SiC/SiC minicomposites are reported. Identical materials are to be irradiated in HFIR to investigating the effects of high-dose neutron irradiation on fiber/matrix interfacial properties, under the DOE-JAEA Phase VI Collaboration Project.

SUMMARY

Tensile properties of unidirectional single tow SiC/SiC minicomposites reinforced with Hi-Nicalon™ Type-S and Tyranno™-SA3 were evaluated. The interphase structure was pyrolytic carbon (PyC) / SiC multilayer and the thickness of the innermost PyC layer was varied (~70, ~240 and ~1150 nm). Only the Hi-Nicalon Type-S minicomposites with ~240 and ~1150 nm-thick PyC interphases exhibited the pseudo-ductile behavior; others reinforced with Tyranno-SA3 and the Hi-Nicalon Type-S composite with 70 nm-thick PyC interphase underwent brittle to near-brittle fracture behavior. The brittle failure behavior for those composites was attributed primarily to the quite low fiber volume fraction (5-10%). The Hi-Nicalon Type-S minicomposites with ~240 nm-thick PyC interphase exhibited ultimate tensile strength equivalent to 79-104% of the fiber bundle strength but only 70-85% of the strength for the ~1150 nm interphase for a given gauge length. Based on the analysis of the hysteresis loops recorded during the tensile loading and unloading sequences, the sliding stress estimated for the ~1150 nm-thick interphase appeared to be about 0.7 times that of the ~240 nm-thick interphase. This shows that both composites satisfied the global load sharing condition, but the composite with the thicker interphase could not achieve its fiber bundle strength, probably due to the lower interfacial sliding stress.

PROGRESS AND STATUS

Introduction

Silicon carbide (SiC) -based ceramics and composites (SiC/SiC) are considered for applications in various components of fusion and advanced fission reactor systems and fuel assemblies, due primarily to their superior irradiation performance and thermo-physical, -chemical, and -mechanical properties [1, 2]. Continuous SiC-fiber, SiC-matrix composites are of particular importance for applications which require reliability, toughness, and near-net shape fabrication.

One focus of irradiation studies of SiC/SiC composites in the past few decades has been determination of the fundamental response of the materials produced with various constituent options and processing routes. Through this effort, composites containing near-stoichiometric SiC fibers and high crystalline SiC matrices produced by chemical vapor infiltration (CVI) or nano-infiltration and transient eutectic-phase (NITE) processes are found to possess acceptable

* Present affiliation: Fusion Structural Materials Development Group, Fusion Research and Development Directorate, Japan Atomic Energy Agency (JAEA), Japan.

irradiation stability. However, a design scheme for the optimum interphase for radiation service remains unresolved due primarily to the lack of understanding of the irradiation effects on the fiber/matrix interfacial properties.

The minicomposite, which is a composite uni-directionally reinforced with a single fiber tow, is an appropriate geometry for evaluating the interfacial properties [3]. The general advantages of the minicomposite approach are as follows: 1) due to its simple uni-directional (UD) fiber architecture, the in-situ fiber strength and interfacial properties can be determined in relatively simple ways [4, 5], and 2) a large number of specimens can be fabricated at low cost in a relatively short time. Moreover, the very small volume of the minicomposite samples is attractive for irradiation studies due to the very high per-unit-volume cost of irradiation and the radiological concerns associated with the evaluation of irradiated material.

Based on the following background, a procedure for evaluating mechanical properties of the SiC/SiC minicomposite samples has been established at Oak Ridge National Laboratory, with the specific consideration of minimizing the personnel exposure during testing of the radiological samples. In the course of the test procedure development, CVI SiC matrix minicomposite samples with single PyC interphase, reinforced with four different near-stoichiometric SiC fibers were evaluated in the unirradiated condition [6]. In this study, the tensile properties of the SiC/SiC minicomposites with PyC/SiC multilayered interphase structure are reported. These materials will be irradiated starting this year under the DOE-JAEA Phase VI Project to investigate the effects of neutron irradiation on F/M interphase microstructure and mechanical properties [7].

EXPERIMENTAL

Materials

Table I describes the minicomposites, and scanning electron micrographs of polished cross sections for each minicomposite are shown in Figure 1. In brief, six types of UD single-tow minicomposites reinforced with two different SiC fibers were prepared in this study. Hi-Nicalon™ Type-S (TypeS) or Tyranno™-SA3 (SA3) fibers were used as reinforcements. The UD minicomposites were fabricated by the CVI process at Hyper-Therm High-Temperature Composites, Inc. (Huntington Beach, California). The fiber/matrix (F/M) interphase consists of five SiC/PyC layer sequences; nominal structure is fiber/e nm PyC/1000 nm SiC/20 nm PyC/1000 nm SiC/20 nm PyC/1000 nm SiC/20 nm PyC/1000 nm SiC/20 nm PyC/matrix, where e is the thickness of the innermost PyC interphase. Three different thickness of e was prepared. Total thickness of the interphase should be 4150-5230 nm Hereafter, the IDs indicated in Table I (TypeS-70, -240, -1150 for Hi-Nicalon Type-S (UD) fiber reinforced CVI matrix minicomposites with e = 70, 240, 1150 nm, and SA3-70, -230, -1000 for Tyranno-SA3 minicomposites with e = 70, 240, 1150 nm) are used.

Table I. Properties of minicomposites used in this study. Nominal mechanical properties of SiC fibers are also listed as supplied by their manufactures.

ID	Fiber	e [nm]	Matrix	r_f [μm]	N [-]	V_f [%]	σ_f [GPa]	E_f [GPa]	ϵ_f [%]
TypeS-70	Hi-Nicalon Type-S	70	CVI	6	500	5-6	2.6	420	0.6
TypeS-240	Hi-Nicalon Type-S	240	CVI	6	500	5-6	2.6	420	0.6
TypeS-1150	Hi-Nicalon Type-S	1150	CVI	6	500	5-10	2.8	420	0.6
SA3-70	Tyranno-SA3	70	CVI	3.75	1600	5-9	2.8	409	0.7
SA3-230	Tyranno-SA3	230	CVI	3.75	1600	5-7	2.8	409	0.7
SA3-1000	TyrannoSA-3	1000	CVI	3.75	1600	5-9	2.8	409	0.7

Table I notations are based on: multilayer structure is fiber/ e nm PyC /1000 nm SiC /20 nm PyC/1000 nm SiC/20 nm PyC/1000 nm SiC /20 nm PyC/1000 nm SiC/20 nm PyC/matrix. e = the thickness of the most inner PyC layer, r_f = the fiber radius, N = the number of filaments in a tow, V_f the fiber volume fraction, σ_f = the single fiber strength at 25 mm, E_f = the Young's modulus of a fiber, and ϵ_f = the fiber elongation.

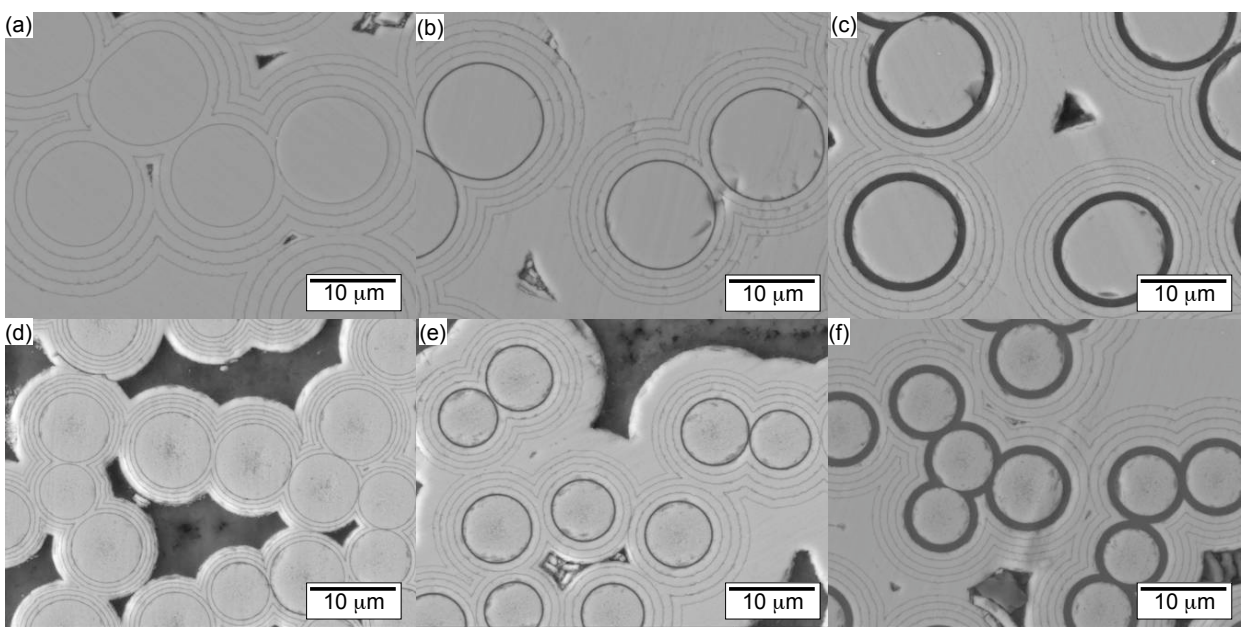

Figure 1. Scanning electron micrographs of polished cross sections of (a) TypeS-70, (b) TypeS-240, (c) TypeS-1150, (d) SA3-70, (e) SA-230 and (f) SA-1000 minicomposites.

Cross sectional area of the minicomposite ($S_c = S_f + S_i + S_m$) and fiber volume fraction (V_f) were calculated from the mass of the fiber bundle, PyC and minicomposite;

$$V_f = \frac{S_f}{S_f+S_i+S_m} = \frac{\pi r_f^2 N}{\pi r_f^2 N + \pi\left((r_f+e)^2 - r_f^2\right)N + \frac{M_c - (M_f + M_i)}{Ld_m}} \quad (1)$$

where S_j is the cross sectional area, r_f the fiber radius, N the number of filaments in a tow, M_j the mass, L the specimen length, and d_j the density. Subscripts f, i, m and c denote fiber, interphase, matrix and composite respectively. M_f and M_i are obtained from $M_f = S_f N L d_f$ and $M_i = S_i N L d_i$. In the calculation, it was assumed that the innermost PyC layer was perfectly deposited around each fiber and that the effect of other four thin PyC layers on mass and density can be ignored. The parameters used in the V_f calculation were listed in Table II. It is noted that all composites in this study have a quite low V_f (only 5-10%).

Table II. The values used in the analysis for fiber volume fraction and ultimate tensile stress.

Symbol	Description	Fiber type	Value	Unit	Ref.
d_f	Density of SiC fiber	(Hi-Nicalon Type-S)	2.98	g/cm^3	[8, 9]
		(Tyranno-SA3)	3.1	g/cm^3	[8, 9]
d_m	Density of SiC matrix		3.21	g/cm^3	[10]
d_i	Density of PyC layer		1.91	g/cm^3	[11]
σ_1	Fiber bundle strength at L_1	(Hi-Nicalon Type-S)	2477	MPa	[8, 9]
		(Tyranno-SA3)	2412	MPa	[8, 9]
L_1	Fiber gauge length		25	mm	[8, 9]
m	Weibull modulus	(Hi-Nicalon Type-S)	6.4	-	[8]
		(Tyranno-SA3)	8.2	-	[8]

Tensile Tests

The test apparatus and specimen preparation are described elsewhere [6]. Tensile tests were conducted using an electromechanical testing machine (Insight 10, MTS Systems Co., Eden Prairie, Minnesota) with a load capacity of 1000 N. Strain was measured by a pair of linear variable differential transducers, LVDTs (Lucas Schaevitz GCA-121-125, Hampton, Virginia). We adopted an alignment system similar to the one used in single fiber tensile testing standardized in ASTM C 1557 in order to assure specimen alignment. The pair of aluminum tabs was fastened to both sides of a minicomposite sample using an epoxy adhesive dispersed by a syringe. The specimen to be glued was fixed in a V-notched fixture with flathead screws for assuring specimen alignment. This fixture including the specimen was cured at 110°C for more than 3 hours in an air furnace in order to develop the adhesive's maximum bonding strength. The gauge length of the specimens is 18 mm, defined by the distance between the inner ends of the aluminum tabs. The specimen was clamped into the simple V-notched fixtures with flathead screws. A guide rail was used to confirm specimen alignment and to avoid damaging the specimen during handling.

The tests were conducted at ambient conditions under crosshead displacement control at 0.05 mm/min. Unloading/reloading cyclic tensile tests were conducted to evaluate interfacial properties. Prior to the tensile tests, compliance of the grip assembly was determined using a set of tungsten wires with varied gauge lengths, and the system compliance of 4.32×10^{-2} μm/N was obtained. Tensile strain (ϵ) is determined by the following equation, $\epsilon = (\Delta L - C_S P)/L_0$, where ΔL the average crosshead displacement recorded by LVDTs, C_S the system compliance, P the applied load, and L_0 the gauge length. The minicomposite tensile stress (σ) is simply defined as $\sigma = P/S_c$. The proportional limit stress (PLS) was defined as the stress at 0.5% deviation from the extrapolated fit of the slope by the least squares method for the initial loading.

The ultimate tensile strength of the minicomposite (UTS, σ_{UTS}) was converted to the fiber-averaged UTS ($\sigma_{\mathrm{U,f}}$) using the equation, $\sigma_{\mathrm{U,f}} = \sigma_{\mathrm{UTS}}/V_{\mathrm{f}}$. This was compared with the fiber bundle strength (σ_{bundle}) in order to know the interaction between effective UTS on fibers and interfacial sliding stress (τ). σ_{bundle} at given length was calculated from the following equation based on the weakest-link theory, assuming that fracture origins of a same fiber is spatially distributed strictly within a volume three-dimensionally [12, 13];

$$\frac{\sigma_1}{\sigma_2} = \left(\frac{V_2}{V_1}\right)^{1/m} = \left(\frac{L_2}{L_1}\right)^{1/m} \tag{2}$$

where σ_j, V_j, L_j, and m are the fiber bundle strength, the volume of the fiber bundle, the gauge length at the condition *j* (= 1 or 2), and the Weibull shape parameter, respectively. The fiber characteristic values reported by Sauder *et al.* [8, 9] were used as a reference shown in Table II.

RESULTS AND DISCUSSION

Tensile Stress-Strain Responses

Representative tensile stress-tensile strain curves are shown in Figure 2 for all six materials. Also, the results of the mechanical properties evaluation are listed in Table III. The TypeS-70, SA3-70 and -1150 composites exhibited brittle behavior with no fiber pull-out observed on the fracture surfaces by optical microscope observation. The SA3-1000 composites have instable fracture behavior; includes both brittle and pseudo-ductile, but fiber pull-out was not confirmed. Only the TypeS-240 and -1150 composites exhibited pseudo-ductile fracture with significant fiber pull-out. Both composites showed significant drop of tensile stress just after their proportional limit (Figure 2 (b, c)). As shown in Figure 3, the Type-S minicomposite with thicker e (-1150) had larger tensile elongation (0.5-0.75% vs. 0.2-0.6% of the TypeS-240) and smaller normalized tensile strength to the fiber bundle strength at given gauge length (70-85% vs. 79-104 % of the TypeS-240). For all six composites, the matrix crack spacing ($\bar{d}$) could not be measured even though the methods by Murakami boiling etching solution and by a crack measurement using replica films were tried.

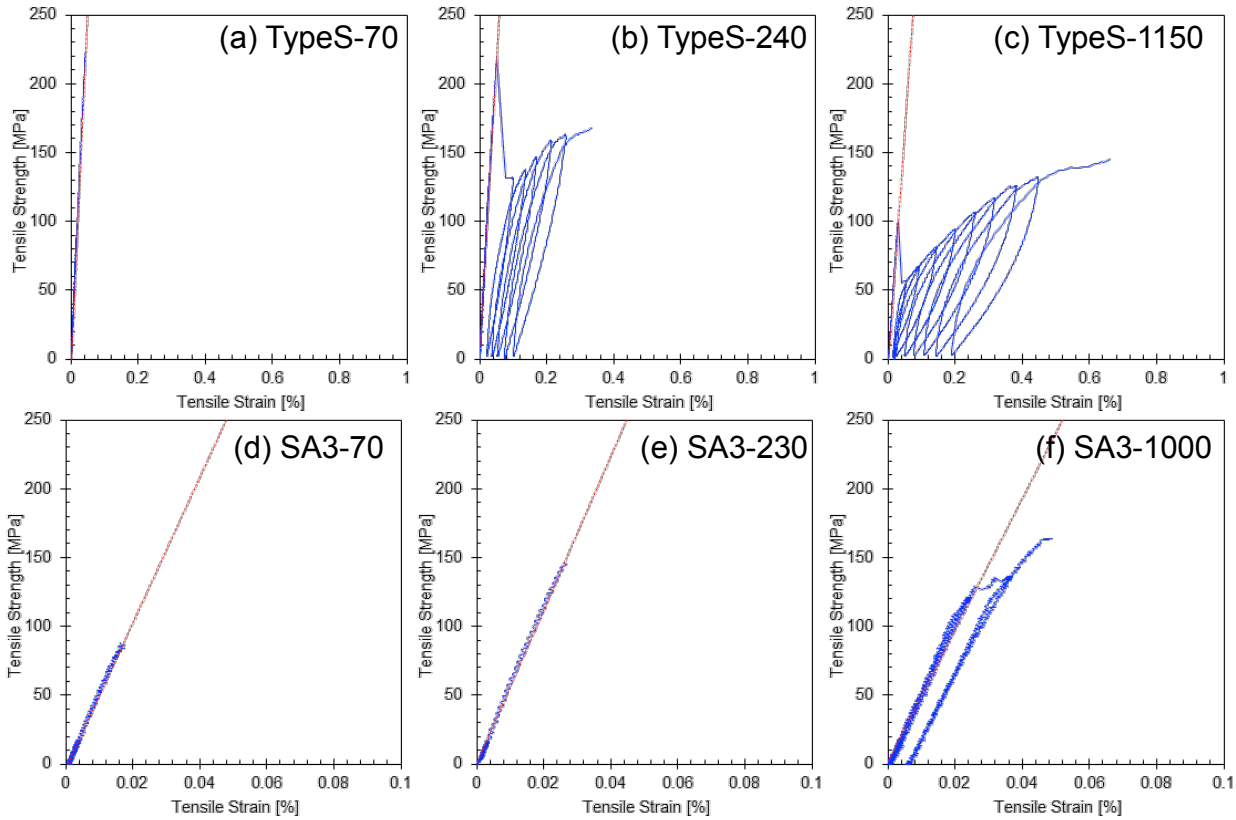

Figure 2. Representative tensile stress-strain curves for (a) TypeS-70, (b) TypeS-240, (c) TypeS-1150, (d) SA3-70, (e) SA3-230 and (f) SA3-1000 minicomposites. Note that the tensile strain axis is different for the Type S and SA3 minicomposites.

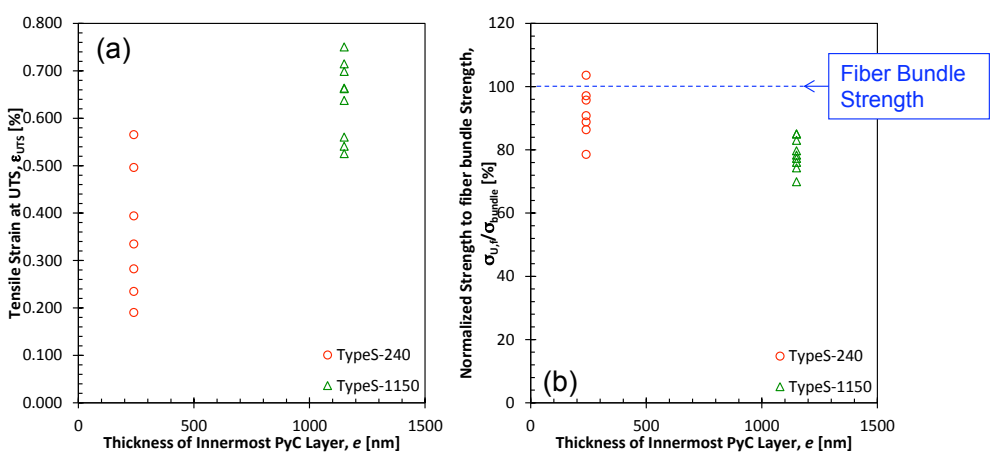

Figure 3. (a) Tensile strain at UTS, and (b) strength normalized to fiber bundle strength of the TypeS-240 and -1150 composites.

Table III. Tensile properties of the minicomposites. Numbers in parenthesis show one standard deviation.

ID	Fiber	e [nm]	Matrix	Fracture Behavior	σ_{PLS} [MPa]	σ_{UTS} [MPa]	ϵ_{UTS} [%]	$\sigma_{U,f}/\sigma_{bundle}$ [%]	#
TypeS -70	Hi-Nicalon Type-S	70	CVI	Brittle	-	164 (80)	0.044 (0.024)	-	3
TypeS -240	Hi-Nicalon Type-S	240	CVI	Pseudo-Ductile	106 (55)	136 (18)	0.357 (0.137)	92 (8)	7
TypeS -1150	Hi-Nicalon Type-S	1150	CVI	Pseudo-Ductile	99 (54)	141 (27)	0.639 (0.080)	79 (5)	9
SA3 -70	Tyranno -SA3	70	CVI	Brittle	-	71 (23)	0.013 (0.005)	-	2
SA3 -230	Tyranno -SA3	230	CVI	Brittle	-	146 (-)	0.026 (-)	-	1
SA3 -1000	Tyranno -SA3	1000	CVI	Brittle	-	199 (42)	0.045 (0.014)	-	4
				Pseudo-Ductile	130 (27)	205 (33)	0.065 (0.012)	-	5

σ_{PLS} = the proportional limit stress of a minicomposite, σ_{UTS} = the ultimate tensile strength of a minicomposite, ϵ_{UTS} = the tensile strain at UTS, $\sigma_{U,f}/\sigma_{bundle}$ = normalized strength to fiber bundle strength, and # = the number of valid tests.

The reasons that almost half of the composites exhibited brittle behavior and that the TypeS-240 and -1150 showed discontinuity in their strain-stress curves at their proportional limit can be reasonably explained by the quite low fiber volume fraction (V_f), although the potential effects of PyC/SiC multilayered interphase structure (4150-5230 nm in total) and fiber surface roughness can also be considered. Under such low V_f condition, cracks could not detect the F/M interphases, and then penetrate the F/M interphase. As a result the composites exhibited brittle behavior with flat fractured surfaces. Based on a simple calculation according to the classical Aveston-Cooper-Kelly theory [14] (the theory by Budiansky *et al.* [15] is suitable for non-slipping interphase, but the ACK theory was chosen due to calculation simplicity), more than 20% fiber volume fraction is estimated as necessary for these minicomposites to exhibit "multiple" fracture [16], which is the behavior of a composite's pseudo-ductility when the fibers will not fail and load transferred to them when the matrix breaks, leading to multiple cracking of the matrix. However the V_f of the minicomposites this study (5-10%) is much smaller than the critical V_f for the "multiple" fracture from the theory. As a result of the preliminary optical microscope observation, any sign of "multiple" fractures (pull-out, matrix crack spacing, etc.) could not be measured this time.

The reason of the discontinuity in TypeS-240, -1150 at their proportional limit in their strain-stress curve is also due to the quite low V_f. It was confirmed that very thick CVI-SiC matrix (around 200-300 μm) was deposited around the fibers, shown in Figure 4. It is reported by Morscher [17] that such thick "sheath" deposition makes it difficult to measure the fiber pull-out length and matrix crack spacing ($\bar{d}$), i.e. to evaluate interfacial sliding stress (τ) directly. Additionally, this

sheath also makes the proportional limit stress more scattered and unsuitable, because the minicomposites without cracks behaves as if they are monolithic material until crack initiates.

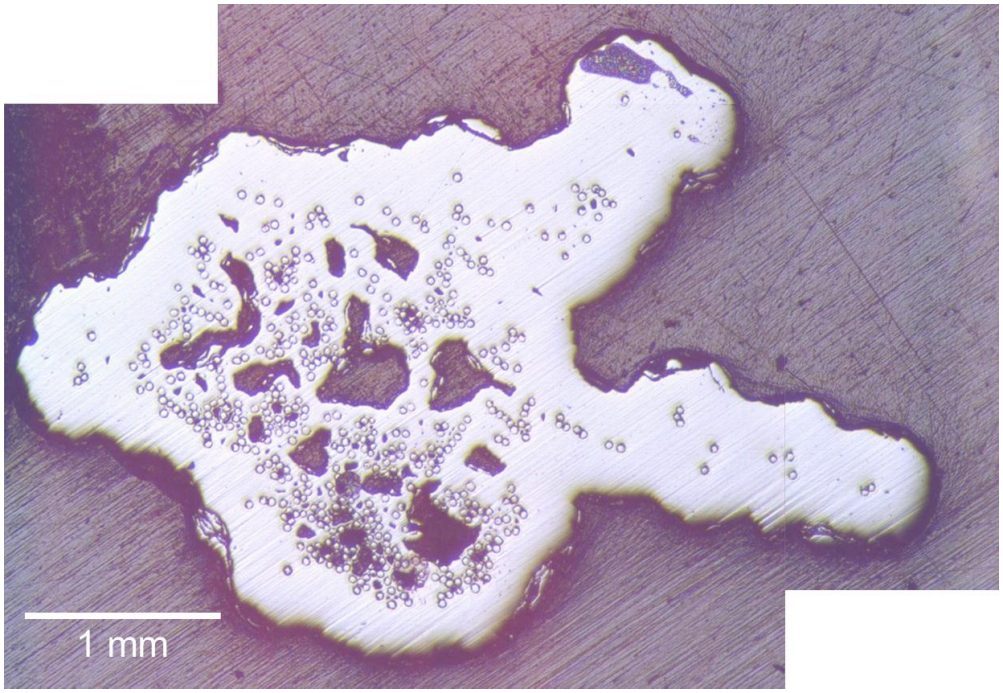

Figure 4. Optical micrograph of cross section of the TypeS-1150 minicomposite with thick CVI coating.

Hysteresis Loop Analysis

In order to know the relationship between τ and in-situ fiber strength, the hysteresis loop analysis was found to be a good tool. Since the $\bar{d}$ could not be experimentally detected due to quite low V_{f}, (i.e. thick "sheath" coating), τ cannot be obtained quantitatively. However, it can be qualitatively estimated from the hysteresis loop analysis, by the following method of Katoh *et al.* [18]. Maximum hysteresis loop width ($\delta\epsilon_{\mathrm{max}}$) is expressed as follows [19],

$$\delta\epsilon_{\mathrm{max}} = \frac{b_2(1-a_1V_{\mathrm{f}})^2\sigma_{\mathrm{p}}^2}{8V_{\mathrm{f}}^2\tau E_{\mathrm{m}}} \cdot \frac{r_{\mathrm{f}}}{\bar{d}} \tag{3}$$

, where σ_{p} is the peak stress, E_i the Young's modulus, $\bar{d}$ the mean matrix crack spacing distance, and a_1, b_2 the Hutchinson-Jensen parameters given by [20],

$$a_1 = \frac{E_{\mathrm{f}}}{E_{\mathrm{c}}} \tag{4}$$

$$b_2 = \frac{(1+\nu)E_{\mathrm{m}}[E_{\mathrm{f}} + (1-2\nu)E_{\mathrm{c}}]}{E_{\mathrm{f}}[(1+\nu)E_{\mathrm{f}} + (1-\nu)E_{\mathrm{c}}]} \tag{5}$$

with ν being Poisson's ratio, assumed to be same and isotropic in fiber and matrix ($\nu_f = \nu_m = \nu$). Also, the matrix damage parameter ($\mathcal{D}$) is defined as [21],

$$\mathcal{D} = \frac{E_c - E^*}{E^*} = \mathcal{B}\frac{r_f}{\bar{d}}\sigma_p^2 \tag{6}$$

where E^* is the elastic unloading modulus at peak stress, and $\mathcal{B}$ a constant. Using this equation, Equation (3) can be rewritten, with K constant, as;

$$\delta\epsilon_{max} = \frac{K}{\tau}\cdot\mathcal{D}\sigma_p^2 \tag{7}$$

Equation (7) indicates that τ can be estimated qualitatively from the slope of a $\delta\epsilon_{max} - \mathcal{D}\sigma_p^2$ plot. Figure 5 shows this analytical result for the TypeS-240 and TypeS-1150 minicomposites. $\delta\epsilon_{max}$ was measured at half of peak stress of each cycle. According to the hysteresis loop analysis, τ of the TypeS-1150 composites is about 0.7 times as the TypeS-240 composites.

The tensile properties of a UD composite system are strongly affected by the Weibull modulus (m), the characteristic strength (σ_0) of the fibers, and the interfacial sliding stress (τ). Under the assumption of global load sharing (GLS) theory [22], the fiber-averaged UTS ($\sigma_{U,f}^{GLS}$) in a unidirectional composite system is expressed as follows:

$$\sigma_{U,f}^{GLS} = \left(\frac{\sigma_0^m \tau L_0}{r_f}\right)^{\frac{1}{m+1}}\left[\frac{2(m+1)}{(m+2)m}\right]^{\frac{1}{m+1}}\left(\frac{m+1}{m+2}\right) \tag{8}$$

with the in-situ fiber bundle strength ($\sigma_{U,f}^{GLS}$), Weibull mean strength (σ_0), the Weibull modulus(m), the gauge length (L_0), and the interfacial sliding stress (τ). Roughly interpreting this equation, $\sigma_{U,f}^{GLS}$ is dependent on only τ. Hence, it is considered that both composites satisfy the global load sharing condition suggested by Curtin [22], but the TypeS-1150 could not achieve its fiber bundle strength compared with the TypeS-240, probably due to the lower interfacial sliding stress.

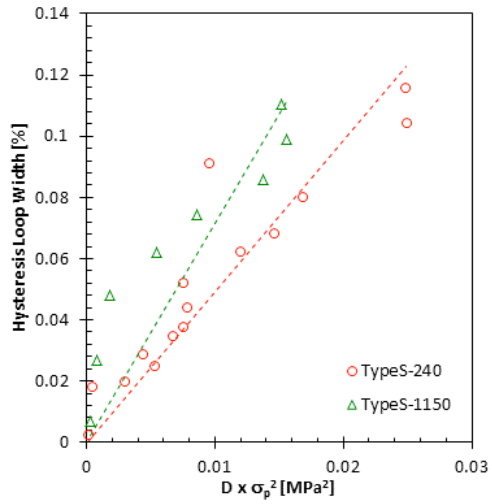

Figure 5. Hysteresis loop width plots against the $\mathcal{D}\sigma_p^2$ values of the TypeS-240 and -1150 minicomposites. It is noted that steeper slope indicates lower τ.

ACKNOWLEDGEMENT

This research was sponsored by the Office of Fusion Energy Sciences, US Department of Energy under contract DE-AC05-00OR22725 with UT-Battelle, LLC.

REFERENCES

[1] T. Nozawa, T. Hinoki, A. Hasegawa, A. Kohyama, Y. Katoh, L. L. Snead, C. H. Henager Jr, J. B. J. Hegeman, *J. Nucl. Mater.* **386-388** (2009) 622.
[2] Y. Katoh, L. L. Snead, C. H. Henager Jr., A. Hasegawa, A. Kohyama, B. Riccardi, H. Hegeman,
J. Nucl. Mater. **367-370** (2007) 659.
[3] R. Naslain, J. Lamon, R. Pailler, X. Bourrat, A. Guette, F. Langlais, Composites *Part A: Appl. Sci. Manuf.* **30** (1999) 537.
[4] J. Lamon, F. Rebillat, A. G. Evans, *J. Am. Ceram. Soc.* **78** (1995) 401.
[5] E. Vagaggini, J.-M. Domergue, A. G. Evans, *J. Am. Ceram. Soc.* **78** (1995) 2709.
[6] K. Ozawa, Y. Katoh, E. Lara-Curzio, L. L. Snead, T. Nozawa, *Ceram. Eng. Sci. Proc.* **31** (2010) 208.
[7] T. Nozawa, K. Ozawa, H. Tanigawa, Y. Katoh, L. L. Snead, R. E. Stoller, Research Plan and Status of High-Dose Rabbit Irradiation Experiment for Silicon Carbide Composites, in these reports.
[8] C. Sauder, A. Brusson, J. Lamon, *Ceram. Eng. Sci. Proc.* **29** (2008) 91.
[9] C. Sauder, A. Brusson, J. Lamon, *Int. J. Appl. Ceram. Technol.* **7** (2010) 291.
[10] From the manufacturer's catalogue,
http://www.dow.com/assets/attachments/business/gt/advanced_ceramics/cvd_silicon_carbide/tds/cvd_silicon_carbide.pdf
[11] Estimated from the PyC oxidation rate of the same minicomposites. C. H. Kim, Y. Katoh, "Active and passive oxidation of CVD-SiC under HTGR operating condition," presented at the

35th International Conference and Exposition on Advanced Ceramics and Composites, (2011).
[12] J. B. Watchman, **Mechanical Properties of Ceramics**, John Wiley & Sons Inc., New York, 1996.
[13] ASTM C 1239-07.
[14] J. Aveston, G. A. Cooper, A. Kelly, The Properties of Fibre Composites: Conference Proceedings, National Physical Laboratory, 4 November (1971) 15.
[15] B. Budiansky, J. W. Hutchinson, A. G. Evans, *J. Mech. Phys. Solids* **34** (1986) 167.
[16] J. Aveston, A. Kelly, *J. Mater. Sci.* **8** (1973) 352.
[17] G. N. Morscher, J. Martinez-Fernandez, *J. Am. Ceram. Soc.* **82** (1999) 145.
[18] Y. Katoh, L. L. Snead, T. Nozawa, S. Kondo, J. T. Busby, *J. Nucl. Mater.* **403** (2010) 48.
[19] A. G. Evans, J. M. Domergue, E. Vagaggini, *J. Am. Ceram. Soc.* **77** (1994) 1425.
[20] J. W. Hutchinson, H. M. Jensen, *Mech. Mater.* **9** (1990) 139.
[21] M. Y. He, B. X. Wu, A. G. Evans, J. W. Hutchinson, *Mech. Mater.* **18** (1994) 213.
[22] W. A. Curtin, B. K. Ahn, N. Takeda, *Acta Materialia* **46** (1998) 3409.